A Wearable Coplanar Vivaldi Antenna (CVA) for Internet of Things (IoT)-Based Toddler Stunting Detection

Nurhayati Nurhayati
Department of Electrical Engineering, Faculty of Engineering, Universitas Negeri Surabaya, Surabaya, Indonesia
nurhayati@unesa.ac.id (corresponding author)

Mohammad As'ad Rosyadi
Department of Informatics, Faculty of Information and Creative Technology, Universitas Internasional Semen Indonesia, Gresik, Indonesia
mohammad.rosyadi@uisi.ac.id

Ahmed J. A. Al-Gburi
Center for Telecommunication Research & Innovation (CeTRI), Fakulti Teknologi Dan Kejuruteraan Elektronik Dan Komputer (FTKEK), Universiti Teknikal Malaysia Melaka (UTeM), Jalan Hang Tuah Jaya, Durian Tunggal, Melaka, Malaysia
ahmedjamal@ieee.org (corresponding author)

Ismaini Zain
Department of Statistics, Faculty of Science and Data Analytics, Institut Teknologi Sepuluh Nopember, Surabaya, East Java, Indonesia
ismaini_z@statistika.its.ac.id

Rina Rifqie Mariana
Department of Culinary Education Study, Faculty of Engineering, Universitas Negeri Malang, Jalan Semarang, Malang, East Java, Indonesia
rina.rifqie.ft@um.ac.id

Annis Catur Adi
Department of Nutrition, Faculty of Public Health, Universitas Airlangga, Surabaya, Indonesia
annis_catur@fkm.unair.ac.id

Nurul Muslihah
Department of Nutrition Science, Faculty of Health Science, Universitas Brawijaya, Malang, East Java, Indonesia
nurul_muslihah.fk@ub.ac.id

Amalia Ruhana
Nutrition Study Program, Faculty of Sports and Health Sciences, Universitas Negeri Surabaya, Surabaya, Indonesia
amaliaruhana@unesa.ac.id

Received: 29 May 2025 | Revised: 23 June 2025, 9 July 2025, and 14 July 2025 | Accepted: 16 July 2025

 DOI: https://doi.org/10.48084/etasr.12430

ABSTRACT

Stunting is a significant health issue affecting the growth of children under five, particularly in developing countries. This study aims to develop a portable stunting detection system integrated with a wearable Coplanar Vivaldi Antenna (CVA) using the Internet of Things (IoT) and an ESP32 microcontroller. The system comprises two components: a hat embedded with ultrasonic and flex sensors for measuring height and head circumference, and a platform equipped with a load cell sensor to measure body weight. The ESP-NOW communication protocol is implemented to enable real-time data synchronization. The CVA is integrated into the hat to enable wireless data transmission via IoT to the receiver unit. A parametric study of the CVA was conducted to investigate the effects of cavity width and corrugation. Simulation results show that a CVA with a cavity radius of 3.5 mm achieves an S_{11} below –10 dB across 1.98–3.76 GHz and 5.27–10.84 GHz, (133.17% bandwidth). Variations in the corrugated structure lead to differences in directivity, with the highest gain observed in CVA type C at 7.858 dBi. CVA type J demonstrates resonances at 2.39 GHz (–35.05 dB) and 5.87 GHz (–28.99 dB). The Specific Absorption Rate (SAR) was measured using a child voxel with a value of 0.279 W/kg. Testing shows high accuracy, with error rates of 0.16% for height, 0.13% for head circumference, and 0.08% for body weight, with a data transmission success rate of 93% up to 20 m. The system also calculates Z-scores based on World Health Organization (WHO) standards.

Keywords-antenna; anthropometric; Internet of Things (IoT); Specific Absorption Rate (SAR); wearable antenna

I. INTRODUCTION

The Internet of Things (IoT) and 5G technology have experienced rapid development in recent years and have gradually become an indispensable component of nearly every aspect of our lives, including smart homes, offices, healthcare, industry, and transportation [1-2]. The concept of interconnected devices has fundamentally transformed daily routines, job-seeking methods, and our interactions with the surrounding environment [3]. The growing interest in smart technologies capable of "connecting everything" presents both opportunities and technological challenges [4]. The increasing adoption of Wireless Body Area Networks (WBANs) in e-health enables medical professionals, caregivers, and families to access accurate, real-time data for continuous health monitoring and diagnostics. In the near future, the trend toward simultaneous use of multiple interconnected devices and sensors will continue to grow. Therefore, these systems must be designed for user convenience and seamless integration [5]. This makes it essential to advance both electronic systems and wearable antenna technologies, as antennas serve as the key front-end components for transmission and reception [6-7].

Previous studies have introduced textile-based antennas supporting Wi-Fi and operating in the 2.4 GHz Industrial, Scientific, and Medical (ISM) band applications [8]. Additionally, wearable antennas face unique challenges due to reduced efficiency caused by electromagnetic absorption in human tissues, as well as issues related to radiation pattern distortion and impedance mismatch. Such antennas are required to satisfy bandwidth, efficiency, and safety criteria while remaining compatible with economical, large-scale fabrication methods. Wearable antennas designed for WBAN communication play a vital role in healthcare [9], movement tracking [10], military applications [11], and more. Such antennas must be easily and effectively integrated into clothing, requiring mechanical robustness and a simplified fabrication process.

Wearable antennas can be implemented in various forms, including handbags, smart clothing, wristbands , shoes, and snap-on buttons [12]. Numerous techniques have been employed to enhance their performance, such as incorporating fractal geometries, and metasurfaces. Researchers have also explored the use of flexible materials like polycarbonate (PC) and Polyurethane (PU) in [13], Polydimethylsiloxane (PDMS) in [14], Kapton polyimide in [15], polyethylene foam in [16], Ultralam 3850 substrate in [17], and denim fabric in [18]. However, many of these substrate materials present challenges: some are difficult to source, others are excessively flexible, and some become problematic to fabricate or fail to conform to the human body when integrated with the antenna radiator.

All wearable antennas exhibit some degree of undesired back radiation, which may be absorbed by human tissues. Research on antenna related Specific Absorption Rate (SAR) reduction has been conducted in [19] using human voxel models and in [20] for military beret applications. Such radiation poses health risks if it surpasses recommended thresholds. Thus, SAR compliance for wearable use must be taken into account and strictly followed. In this study, we implement wearable textile antennas for IoT-based stunting detection applications.

Stunting is a serious public health issue, particularly in developing countries, with significant long-term impacts on individuals and broader social and economic development. Stunting is defined as impaired child growth resulting from chronic malnutrition, often beginning during pregnancy and continuing until the age of five. Thus, stunting is not only a health issue but also a persistent challenge that affects education, economic development, and overall child welfare. Early detection of stunting plays a crucial role in mitigating long-term consequences. The World Health Organization (WHO) recommends regular monitoring of child growth and development, along with appropriate follow-up actions for any deviations from expected growth standards. One widely used method for early detection is Z-score analysis, a statistical approach that evaluates child growth based on anthropometric parameters such as height, weight, head circumference, and arm circumference. Through Z-score analysis, healthcare providers can easily identify children at risk of stunting and

take appropriate action [21]. Proper nutrition forms the foundation for optimal child development. Despite the existence of conventional diagnostic tools, the high cost, large size, and limited availability of such equipment in remote or under-resourced areas remain major barriers to effective stunting detection and intervention [22]. Therefore, a portable, efficient, and affordable solution is necessary to rapidly collect and analyze relevant data.

This study presents a portable stunting detection system based on the ESP32 microcontroller for early diagnosis and nutritional status assessment. The system comprises a sensor-equipped hat for measuring head circumference and height, and a portable scale for measuring body weight. These components communicate via ESP-NOW, a peer-to-peer communication protocol utilizing MAC addresses for real-time data synchronization. Collected data are transmitted to a cloud server for Z-score analysis. This innovation is expected to significantly improve the detection of stunting risk, particularly in rural areas, where limited resources and inadequate tools often hinder manual Z-score calculations and nutritional evaluations for children [23, 24]. Moreover, the system's compact and user-friendly design allows for deployment in various settings, promoting greater awareness and continuous monitoring of children's stunting status. This study aims to design and implement a textile-based Coplanar Vivaldi Antenna (CVA) for IoT-based toddler stunting detection. A parametric study is conducted on the textile antenna, focusing on cavity radius variation and corrugation shape, to achieve operation at 2.4 GHz and 5.8 GHz with a wide bandwidth. In addition, a SAR analysis is performed, and the textile antenna is directly integrated into a wearable hat to transmit stunting-related data parameters via IoT.

As illustrated in Figure 1, the system comprises a sensor-integrated hat equipped with a flex sensor for measuring head circumference, an ultrasonic sensor for measuring height, and a portable scale for body weight measurement. All devices are connected via an ESP32 microcontroller using ESP-NOW technology for real-time peer-to-peer communication. The collected data are transmitted to a cloud server for analysis, including Z-score calculation and nutrition recommendations using the Weighted Product method. The analysis results are accessible to parents or healthcare professionals through a responsive web interface, enabling practical and efficient early detection of stunting, particularly in regions with limited access to healthcare services.

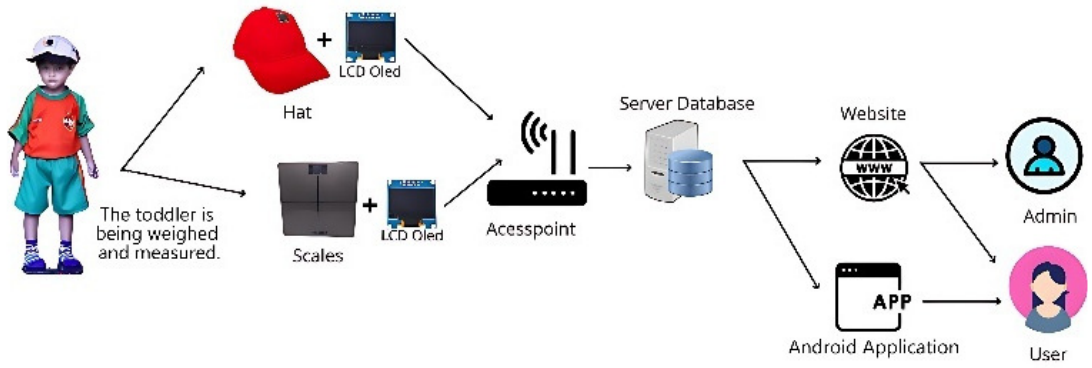

Fig. 1. The architecture of an ESP32-based early stunting detection system.

The key advantage of this innovation, compared to conventional tools, lies in its simple, portable, and efficient design, with the ability to function without requiring an internet connection. This capability not only facilitates the identification of children at risk of stunting but also promotes public awareness of the importance of monitoring children's nutritional status.

This study provides the following research contributions:

- We developed a wideband, dual-band wearable textile antenna that operates in the ISM frequency bands of 2.4 GHz and 5.8 GHz, using felt and super-shield materials in a compact form factor. In contrast, several previously published wearable antennas are relatively large, do not operate in the ISM bands, and exhibit narrow bandwidths.
- The antenna radiator was studied, including the effects of changing the radius of cavity and corrugation shape on the operational frequency and antenna gain. Furthermore, to guarantee safety compliance, the antenna's SAR was assessed using a voxel-based model of the human body.
- This antenna is integrated with sensors for IoT-based stunting detection, which enables transmission of head circumference and height data via a wearable cap, along with weight measurements, and is integrated with Z-score calculations.

II. ANTENNA AND SYSTEM ARCHITECTURE

A. Antenna Configuration

In this study we designed the Vivaldi antenna using flexible material, namely felt which has permittivity of 1.34, tangent delta of 0.02, and substrate thickness of 1 mm, and using a radiator patch using a super shield which has electric conductivity of 1.18×10^5 S/m and a thickness of 0.017 mm. Figure 2 depicts the antenna design, whereas Table I shows its dimensions. CVA is a microstrip antenna that has two tapered slots on the same side, whereas the opposite side is the antenna feeder. The slope of the tapered slot follows (1).

$$y = C_1 e^{Rx} + C_2, \quad C_1 = \frac{y_2 - y_1}{e^{Rx_2} - e^{Rx_1}},$$
$$C_2 = \frac{y_1 e^{Rx_2} - y_2 e^{Rx_1}}{e^{Rx_2} - e^{Rx_1}} \quad (1)$$

where y is the tapered slot curve, and x_1, y_1, x_2, and y_2 are the points where the slope of the tapered slot starts and ends [25].

TABLE I. ANTENNA DIMENSIONS

Parameter	Dimensions (mm)	Parameter	Dimensions (mm)
a	40	m	14.75
b	60	n	30
c	35	o	125
d	10	p	5.95
e	2	q	6
f	17	r	4
g	9	s	5
h	13	t	4.5
i	7.25	u	2.5
j	4	v	2.5
k	22.75		
l	7		

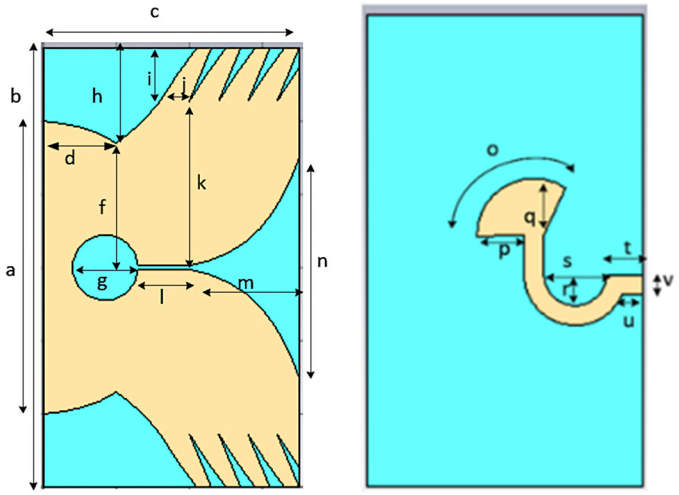

(a) (b)

Fig. 2. Antenna design: (a) front view, and (b) back view.

B. Hardware Components

The measurement system in this study consists of two main instruments: a device for measuring height and head circumference in the form of a baseball cap, and a body mass measuring device in the form of a scale. Both devices are designed in a portable format using ESP-NOW peer-to-peer data transmission technology. The ESP-NOW protocol enables direct communication between two ESP microcontrollers without the need for Wi-Fi connectivity, with data transmission occurring via MAC Address. This technology offers relatively high transfer speeds, with a latency of less than 100 ms and a maximum range of 20 m for 100% success rate [26].

As shown in Figure 3, the anthropometric data measurement system consists of two main components. The first component, as depicted in Figure 3(a), is a portable hat equipped with an ultrasonic sensor to accurately measure the child's height. This sensor works by calculating the time taken for sound waves to bounce back from the surface of the child's head. Additionally, the hat is fitted with two flex sensors used to measure head circumference, with the sensors positioned around the flexible hat rim to adjust to the shape of the child's head.

The measurement results are displayed in real-time on an OLED screen before being sent to the cloud server. The hat uses a LiPo 1S 2,250 mAh battery as its power source, along with a Mini UPS Step-Up Boost module for battery charging and step-up voltage to 5 V DC. All the electronics on the hat are controlled by the ESP32. Figure 3(b) shows a portable scale equipped with a load cell and an HX711 module to accurately measure the child's weight. The HX711 module acts as a signal amplifier to read the output from the load cell and convert it into digital data. Like the hat, the scale also displays the measurement results in real-time on an OLED screen before sending the data to the cloud server. The scale system uses a LiPo 1S 2,250 mAh battery as its power source and a Mini UPS Step-Up Boost module for battery charging and voltage regulation. The ESP32 is used as the main controller in the scale system.

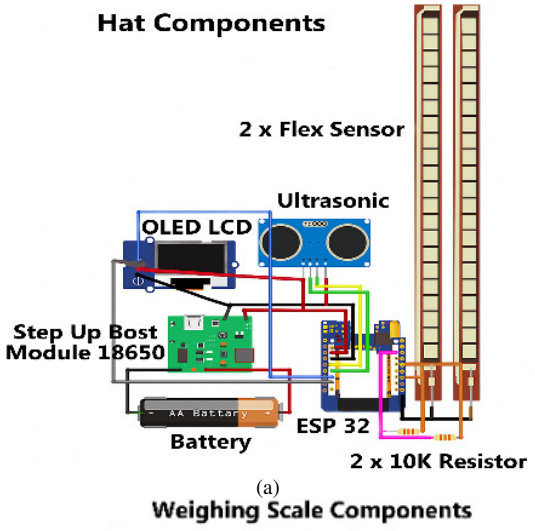

(a)

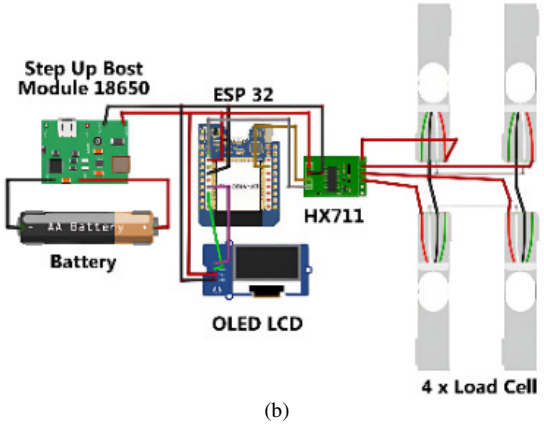

(b)

Fig. 3. Schematic circuit of the: (a) height and head circumference measurement system using a hat, and (b) weight weighing system.

Both systems utilize the ESP-NOW communication protocol, which allows the ESP32 devices to exchange data in a peer-to-peer manner without requiring Wi-Fi network infrastructure. This protocol leverages the devices' MAC addresses for identification, ensuring that sensor data can be transmitted directly to the central control ESP32. This communication ensures real-time data synchronization with very low latency.

Data security is implemented via a RESTful API utilizing the HTTP POST method, secured with TLS (HTTPS), and employs OAuth2 token authentication to guarantee that only authorized devices can contact the server. Simultaneously, communication among local devices employs the ESP-NOW protocol with AES-128 encryption in CCMP mode, utilizing a Pre-Shared Master Key (PMK) to generate a unique Local Master Key (LMK) for each device, thereby ensuring the secrecy, integrity, and authenticity of the communication.

C. Hardware Architecture Design

A device for measuring height and head circumference is designed in the form of a modified hat, sized appropriately for toddlers aged 0–5 years (head circumference 40–57 cm). The hardware architecture is shown in Figure 4. The hat measures 15 cm tall, 25 cm long, and 10 cm wide. To measure toddler head circumference, the flex sensor is inserted inside the hat. When worn, it senses hat curvature changes to accurately measure head circumference. The front of the hat has an ultrasonic sensor that assesses the toddler's height. The ESP32 microcontroller processes sensor data and sends measurement results via peer-to-peer communication. The OLED display performs measurement results in real-time before the data are transmitted to the cloud. A LiPo 1S battery (2,250 mAh) is the power device and is equipped with a Mini UPS Step-Up Boost module for recharging and increasing voltage to 5 V DC. These components create a portable, accurate apparatus for real-time anthropometric data measuring in toddlers, enabling stunting detection. The load cell sensor and HX711 module are used to measure weight with IoT.

D. Software Architecture

The Z-score is calculated based on the anthropometric data collected, such as weight-for-age, height-for-age, and weight-for-height. This calculation compares the child's data with the WHO growth standards using (2) [27]:

$$Z = \frac{x - \mu}{\sigma} \quad (2)$$

where x is the child's data (e.g., height), μ is the mean of the reference population, and σ is the standard deviation of the reference population. The Z-score results are used to determine the child's nutritional status, such as undernourished, malnourished, well-nourished, or overnourished. The software architecture is designed to support data collection, processing, and analysis. The process begins when the toddler wears the sensor-equipped hat and stands on the scale. Meanwhile, the administrator accesses the website to verify measurement results. Users are required to log in by entering their email and password. If the email is not found, the system displays the message "Not Registered." If the email exists but the password is incorrect, a notification stating "Incorrect Email/Password" appears. If both credentials are correct, the user is directed to the dashboard.

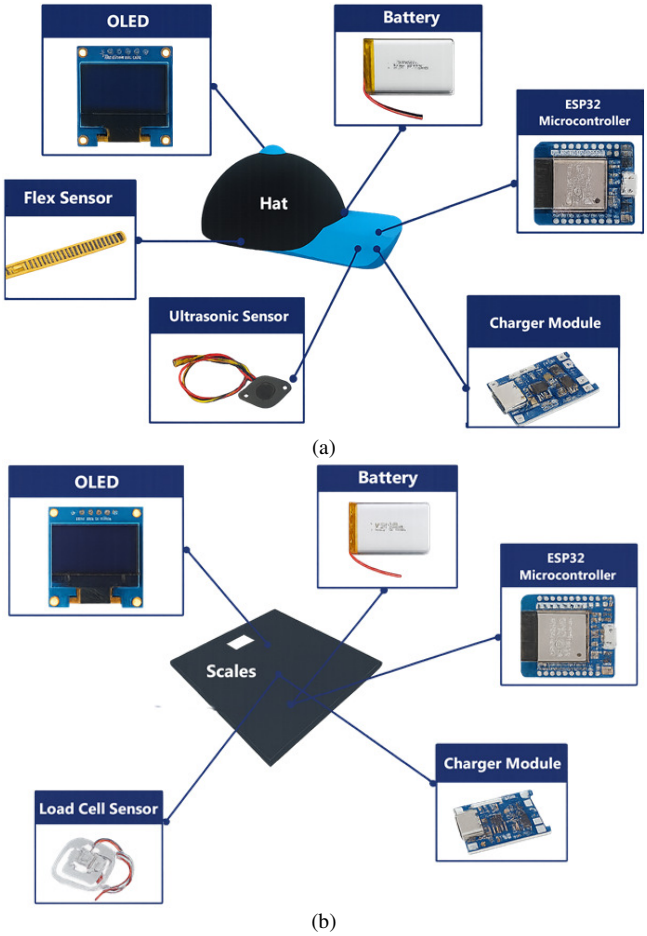

Fig. 4. Architecture of the: (a) hat hardware, and (b) body weight scale.

Before proceeding with measurements, the parent and toddler data must be registered via the "Add Parent" and "Add Toddler" pages. At this stage, users input the parent's information, such as name and email, followed by the toddler's data, including name, date of birth, and other details. This information is then stored in the database. The measurement results are analyzed to calculate the Z-score, total calorie requirements, Basal Metabolic Rate (BMR), and food recommendations based on WHO standards. The system algorithm can be described as follows.

```
Algorithm 1: Stunting Detection Process
Input : Measurement data (height, head
circumference, weight) and the child
database.
Output: Z-score data, nutritional status,
and report files in Excel and PDF formats.
1. The ultrasonic sensor measures the
   height.
2. The flex sensor on the portable hat
   measures the head circumference.
3. If height > 10 cm then:
```

Send height and head circumference data via ESP-NOW to the scale device.
4. Else:
   The device enters sleep mode.
5. The scale receives data and measures the weight using a load cell sensor.
6. If weight > 5 kg then:
   Send the measurement data (height, head circumference, weight) to the cloud server using the POST method.
7. Else:
   The device enters sleep mode.
8. The interface prompts the user to select the child's name from the child database.
9. If the name is found then:
   Link the measurement data with the selected child's ID.
10. Else:
    Display an error message: "Name not found in the database."
11. Calculate the Z-score based on the following data:
    Length-for-Age (L/A), Height-for-Age (H/A), Weight-for-Age (W/A), Weight-for-Length (W/L), Weight-for-Height (W/H), Body Mass Index-for-Age (BMI/A), Head Circumference-for-Age (HC/A)
12. If the measurement value < median then:

$$Z_{score} = \frac{Measurement\ value - Median\ value}{Median\ value - (-SD)}$$

13. Else:

$$Z_{score} = \frac{Measurement\ value - Median\ value}{(+1SD) - Median\ value}$$

14. Determine the nutritional status based on WHO thresholds: Normal, Risk of Stunting, or Severe Stunting.
15. Calculate the child's daily calorie needs (BMR, TDEE) based on anthropometric data and activity factors:
    - BMR for boys/girls aged 0-6 years.
    - Total Daily Energy Expenditure (TDEE).
16. Determine daily calorie requirements based on WHO distribution (carbohydrates, protein, fat).
17. Calculate food recommendations using the Weighted Product method:

    S vector: $S = \prod_{j=1}^{n} \left(X_{i_j}^{w_j} \right)$

    V vector: $V = \frac{S_i}{\sum S}$

    Rank food menus based on the V value.
18. Display the calculation results (Z-score, nutritional status, and food recommendations) on the user interface.
19. Export the report to Excel and PDF format.
20. End of algorithm

III. RESULTS AND DISCUSSION

A. Antenna Performance

We conducted a parametric study on the CVA by varying the radius of the cavity and providing a corrugated structure on the antenna radiator to determine the changes in the performance of the reflection coefficient and directivity of the antenna. The parametric study was conducted by maintaining the shape of the feeding, the size of the substrate, and the bottom shape of the antenna radiator. From the simulation results shown in Figure 5, it is found that changing the cavity radius can change the antenna resonance frequency. For antennas with a radius of cavity (rcav) of 2.5 mm, the best resonance frequency occurs at 5.45–10.46 GHz with an S_{11} minimun of -55.7 dB. With an rcav of 2.5 mm, the antenna has a very wide bandwidth, operating at frequencies of 1.79–3.84 GHz and 5.36–10.74 GHz. At rcav = 3.5 mm the antenna works at a frequency of 1.98–3.76 GHz with S_{11} of -28.25 dB at a frequency of 2.58 GHz. The second band is 5.27–10.84 GHz. At rcav = 4.5 mm, resonance occurs at 2.09–3.8 GHz with a low S_{11} of -42.75 dB at 2.69 GHz and a second resonance at 6.11 GHz with -41.06 dB. With an rcav of 5.5 mm, resonance occurs between 2.83 and 5.8 GHz. The difference in directivity with cavity alterations is small. The highest gain is 7.261 dBi for rcav = 5.5 mm at 7 GHz and 6.69 dBi for rcav = 1.5 mm. Furthermore, to get resonance at 2.4 GHz and 5.8 GHz we use an rcav of 4.5 mm by doing corrugated variations as shown in Figures 6 and 7.

Figure 6 shows the results of S_{11} due to the corrugated variation indicated by the CVA type A-E. In CVA-type A, the best resonance occurs at frequencies of 3.39 GHz (-17.11 dB) and 6.27 GHz (-36.63 dB), whereas in CVA-type B, the resonance frequency is at 3.28 GHz (-30.16 dB) and at 6.18 GHz (-30.08 dB). In CVA type C, resonance is formed at 3 GHz (-49.1 dB) and at 6.18 GHz (-28.45 dB). In CVA type D, resonance occurs at 2.67 GHz (-42.553 dB) and at 6.11 GHz (-40.5 dB). In CVA type-E, resonance occurs at 2.42 GHz (-32.9 dB) and 5.95 GHz (-27.93 dB). By giving a corrugated structure, there is a difference in the directivity produced, especially at frequencies above 3 GHz. However, at frequencies of 1 and 2 GHz, the change is not too significant. At a frequency of 3 GHz, CVA type E has a directivity of 3.93 dBi, whereas CVA type B has a directivity of 0.572 dBi, resulting in an increase in directivity of 3.358 dBi. At a frequency of 6 GHz, CVA type B has a directivity of 6.05 dBi and CVA-type E has a directivity of 3.93 dBi. This indicates that the provision of different corrugation structures on types B and E can increase directivity by 2.12 dBi. At a frequency of 7 GHz, type C has the highest directivity of 8.01 dBi.

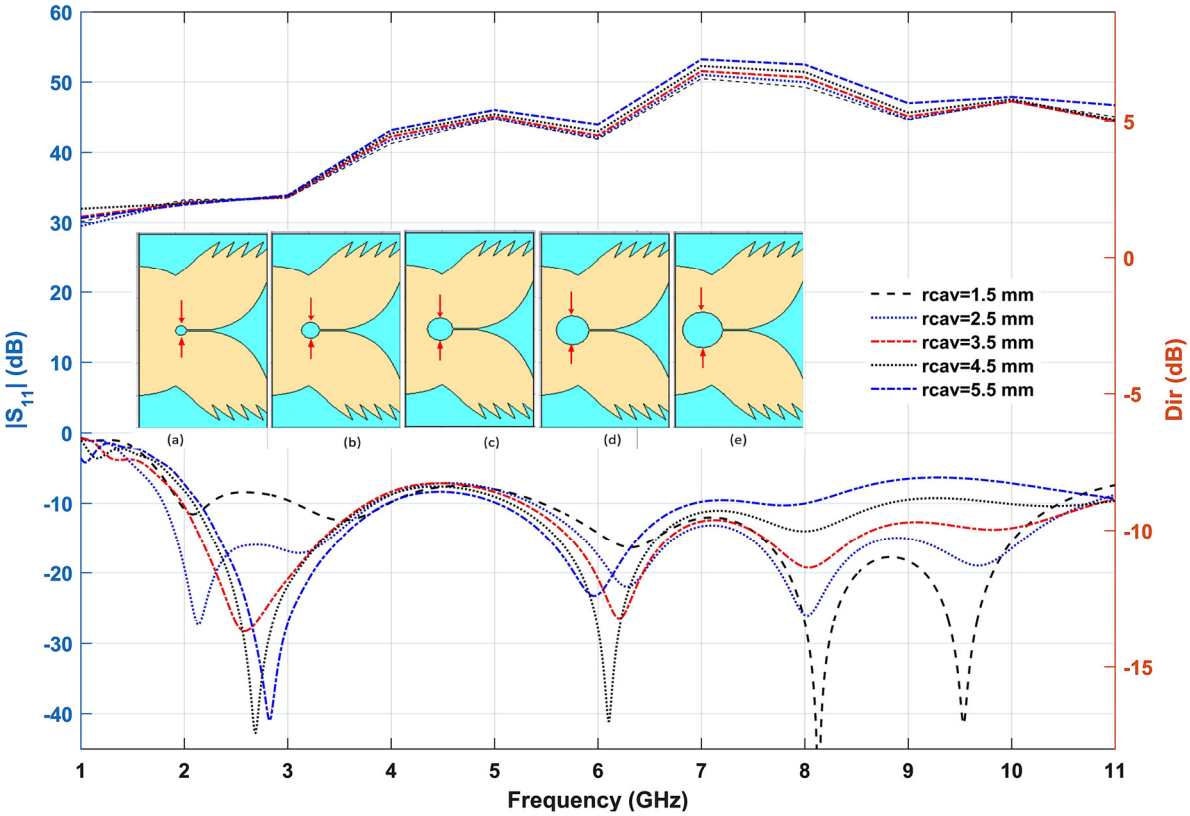

Fig. 5. S_{11} and directivity results for CVA with with cavity width variations.

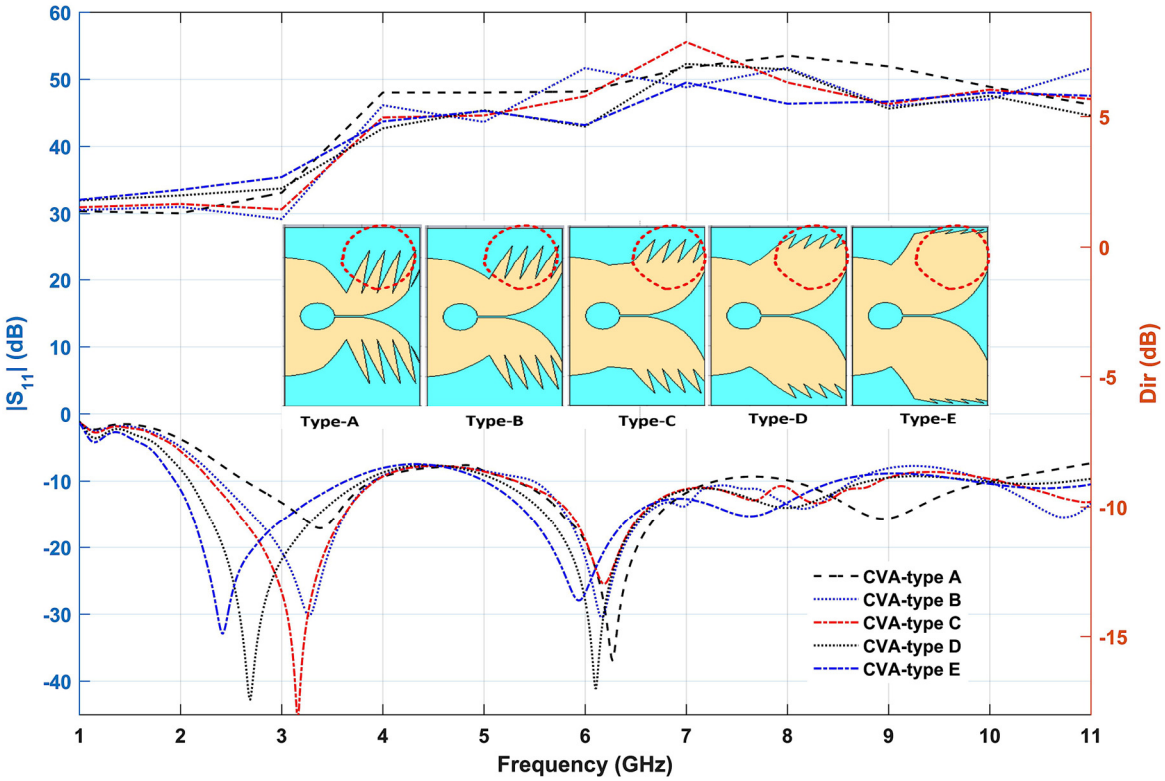

Fig. 6. Simulation results of S_{11} and directivity for CVA with corrugated variations (types A-E).

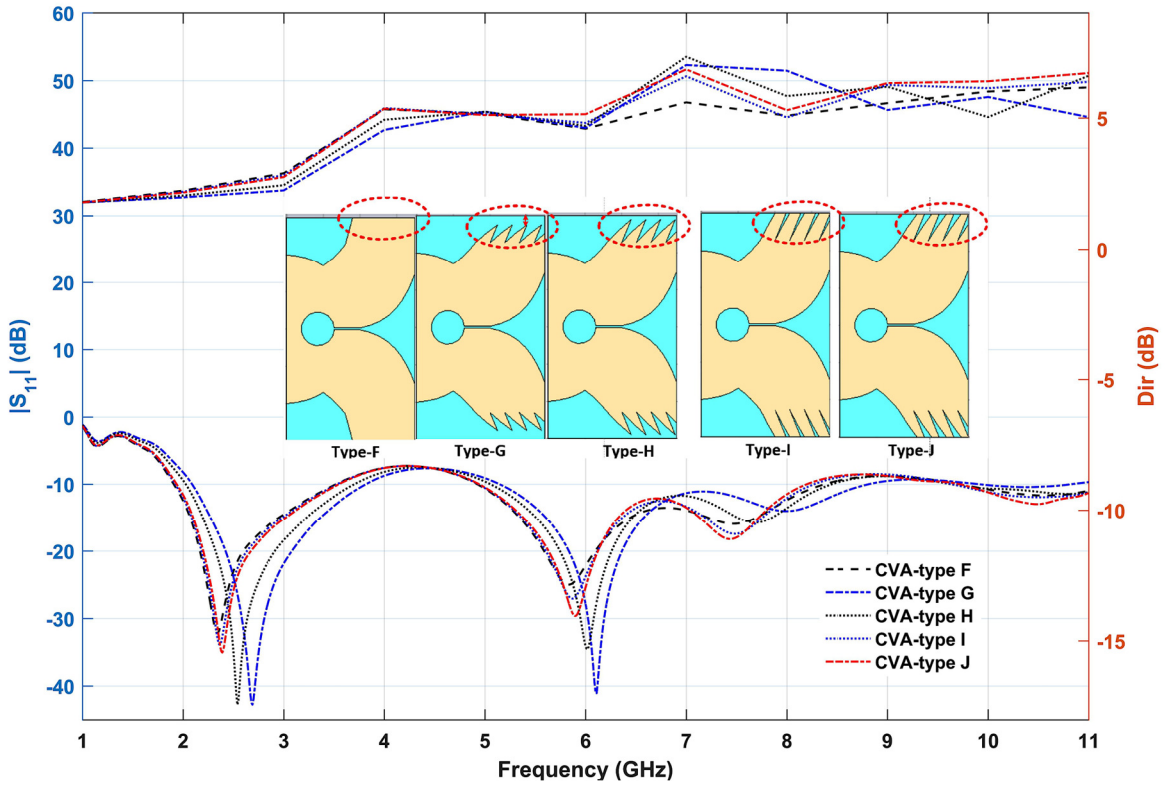

Fig. 7. S_{11} and directivity simulation results for CVA with corrugated variants (types F-J).

By providing a deep corrugated structure, directivity can be increased at several high frequencies, and vice versa. Figure 7 shows CVA type F, G, H, I and J. CVA type F produces resonance at frequencies of 2.34 GHz(-32.21dB) and 5.85 GHz(-25dB), whereas CVA type G produces resonance at 2.69 GHz (-42.51 dB) and 6.09 GHz (-39.7dB). CVA type H produces resonance at 2.54 GHz-41.34 dB) and at 6.02 GHz (-34.12dB). CVA type-I produces resonance at frequencies of 2.36 GHz (-33.23 dB) and 5.87 GHz (-26.86 dB) and CVA type J produces resonance at 2.39 GHz (-35.05 dB) and 5.87 GHz (-28.99 dB), with a percentage of impedance bandwidth of 58.7%.

The CVA types F-J exhibit identical directivity at 2 GHz, as shown in Figure 7. At 7 GHz, the CVA type-H achieves a directivity of 7.33 dBi, whereas type-F reaches 5.59 dBi, an improvement of 1.74 dB. The wavy antenna can change its resonance frequency and directivity, especially at high frequencies.

In this study, SAR testing using CST MWS was conducted on a head phantom to determine the safety limits of the influence of electromagnetic radiation. In this study, the antenna will be tested by placing it behind the head as shown in Figure 8. The voxels consist of bone, brain, eye, mucosa, muscle, fat, nerve, skin, thyroid, and trachea, each with its own voxel data. The SAR value derived from the simulation results is compared to the Federal Communications Commission (FCC) and International Commission on Non-Ionizing Radiation Protection (ICNIRP) requirements, which require a maximum SAR value of 1.6 W/kg per 1 g of tissue mass and 2 W/kg per 10 g. Based on the simulation results, the antenna has a SAR value of 0.279 W/kg at a frequency of 2.4 GHz for 10 g of tissue mass.

Figure 9 shows a comparison of simulation results and measurement results, and it indicates the antenna can work at 2.4 and at 5.8 GHz. Losses from improper connectors or cables may cause measurement differences. The feed point or patch is also somewhat off-design during manufacture and placement. Precision is required for radiator integration and textile substrate feeding. Certain abilities are required when soldering connections to textile materials, since the heat from the soldering iron can damage the textile material. However, the measurement results show that the antenna still meets the expected frequency.

Figure 10 explores the front and back views of the fabricated antenna. Figure 11 shows the integration of electronics on the hat and antenna testing after being integrated into the sensor, Tx module. For this test, the hat was placed on the head using several mannequin models that have several different head circumferences and heights. From the test results, it was obtained that the head circumference, body height, and weight data can be sent to the HP server within 5–7 ms. The stunting detection hat prototype is equipped with a flex sensor to record head circumference and an ultrasonic module for height detection. The test results indicate that the ultrasonic module recorded a mean error rate of 0.16%, whereas the flex sensor reported a typical error margin of 0.13%. The measurement differences between the portable device and manual methods are minimal, demonstrating the reliability of the device in anthropometric data measurements. The hat uses a 1S LiPo battery with a capacity of 2,250 mAh and a total

power consumption of 216.5 mA. However, there is an issue with the device: when the battery voltage reaches 3.3 V, the height measurement becomes unstable. The device's power consumption includes the ESP32 (160 mA), the HX711 module (1.5 mA), and the OLED display (25 mA). The ESP32 microcontroller is powered by a 1S Li-Po battery, which is raised to 5 V via an MT3608 boost converter with feedback resistors R1 = 110 kΩ and R2 = 15 kΩ. Additionally, the ESP32 generates 3.3 V for the sensor, regulated by a 100 µF electrolytic capacitor to prevent load spikes. The device has a power-saving sleep mode. With a standard deviation of 5 ms, the line-of-sight transmission time averaged at 82 ms. Transmission times were stable at 78–85 ms under ideal conditions.

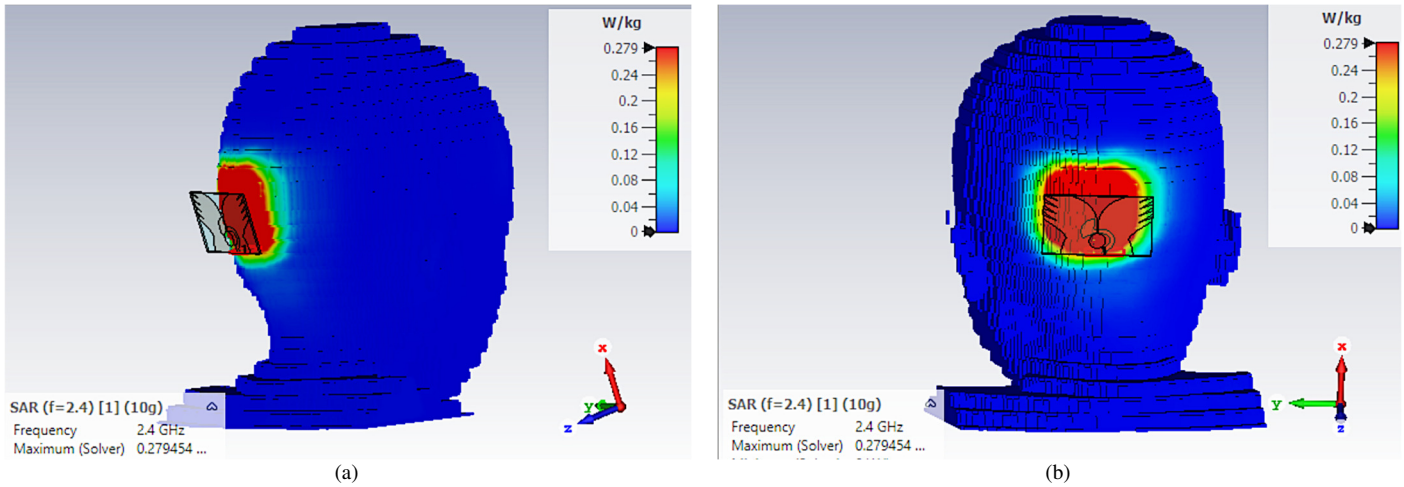

Fig. 8. SAR simulation results for CVA on head phantom: (a). perspective view, and (b) back view.

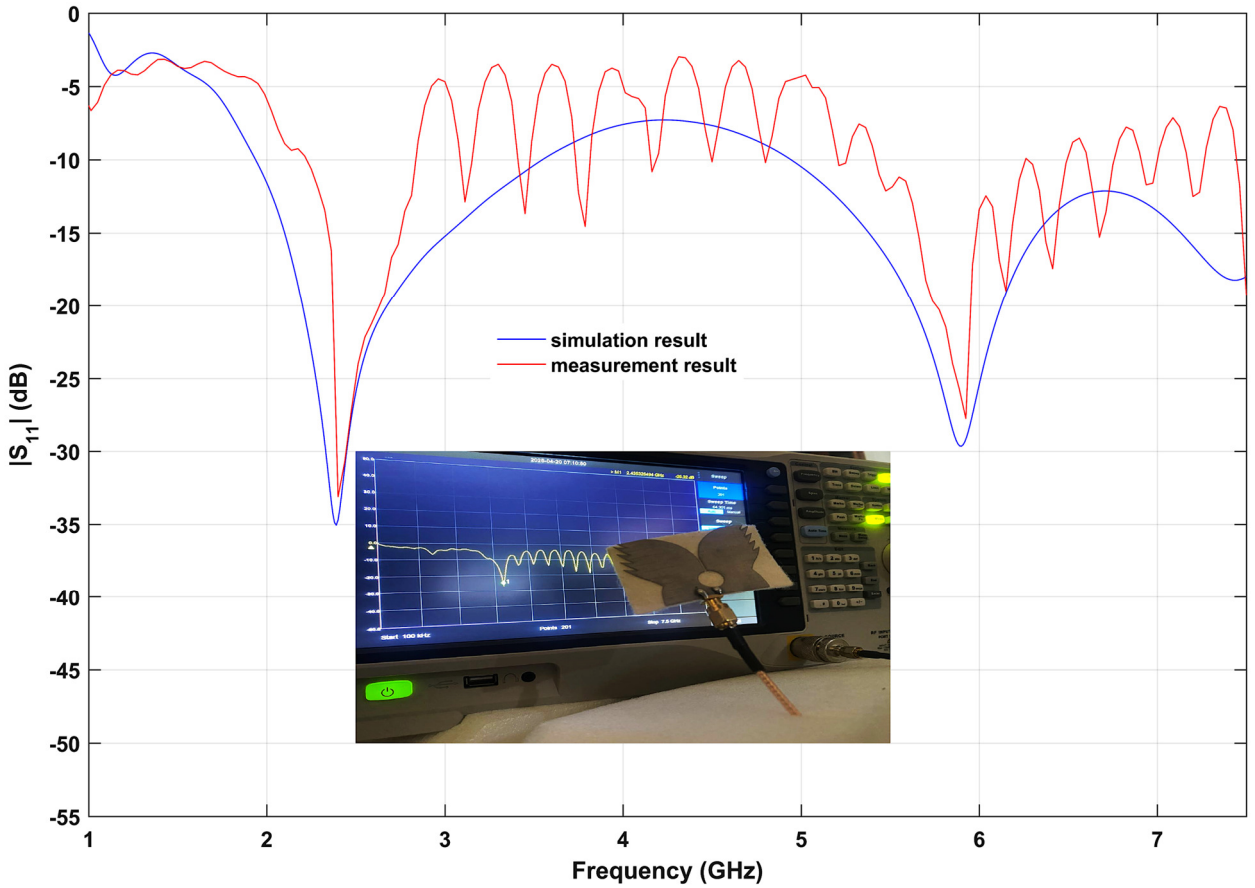

Fig. 9. Comparison of simulated and experimental S_{11} results.

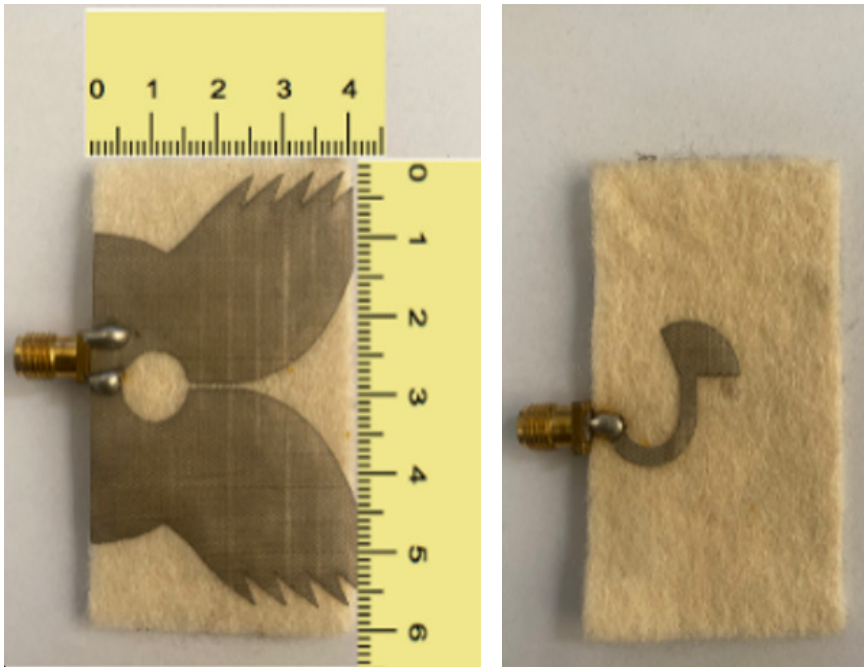

(a) (b)

Fig. 10. Fabricated antenna: (a) top view, and (b) back view.

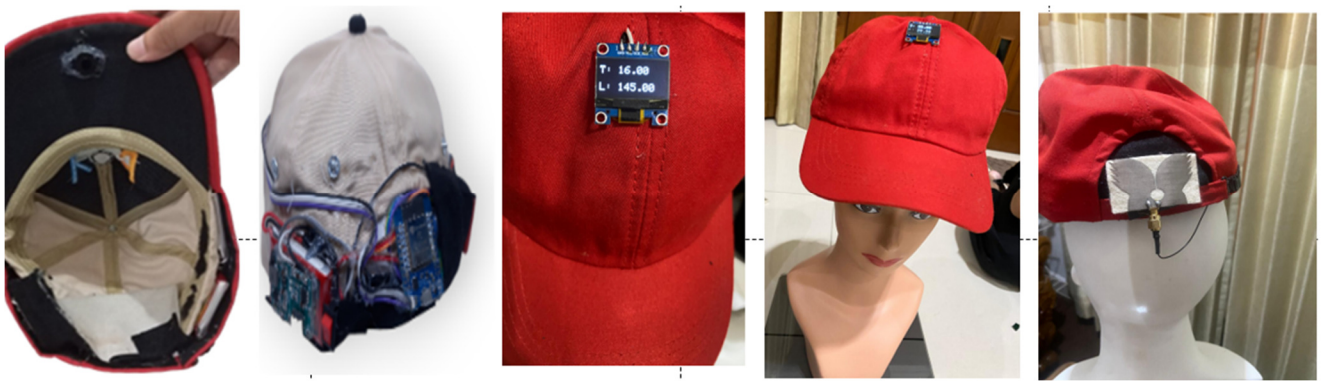

Fig. 11. Electrical components of the hat.

Under physical obstructions, the transmission delay increased to 117 ms, with standard deviation of 7 ms. Transmission was 110–124 ms and suitable for real-time applications. The connection stability was measured by measuring packet delivery over 1–20 m. In line-of-sight conditions, packet delivery was 100% up to 15 m. At 20 m, signal loss and attenuation lowered the delivery success to 93%. Despite physical obstacles, the success rate reached 100% up to 10 m. At 15 m, the success rate dropped to 97%, and at 20 m, to 85%. ESP32 devices consumed 180 mA on average while transferring data, with a range of 175 mA to 185 mA and a standard variation of 5 mA.

In addition, the ESP32's sleep mode reduced power consumption to an average of 10 mA, with a range of 9 mA to 11 mA and a standard deviation of 1 mA. This shows that the system can handle power-efficient applications, especially battery-powered IoT devices. This technique generated accurate anthropometric data in testing. The system is capable of collecting measurement data such as height, weight, and head circumference.

Table II presents a comparison between the proposed antenna and other antennas operating at frequencies around 2.4 GHz. As illustrated in the table, several antennas operating at this frequency still use non-flexible/rigid materials, such as FR-4. Although FR-4 material is inexpensive and readily available, its rigid shape prevents it from bending and being used on curved surfaces. This makes it uncomfortable for use in wearable technology. Softer materials like PTFE, which is included in the table, are more expensive and harder to find. Compared to the textile-based antennas shown in the table, such as jeans and felt, our antenna demonstrates a smaller physical size. Additionally, the proposed antenna offers a broader bandwidth, improved S_{11} performance, and higher gain in relative to analogous antennas operating at around 2.4 GHz.

TABLE II. COMPARISON OF PROPOSED ANTENNA WITH RELEVANT REFERENCES

Ref	Dimensions (mm^2)	Material	Frequency (GHz)	Min S_{11} (dB)	Gain (dBi)	Application
[27]	30 × 45	FR-4	2.4 / 5.8	-30	3.09 / 0.64	WBAN
[28]	38.48× 47	FR-4	2.4	-23.9	4.01	IoT
[29]	40 × 70	Jeans	2.4 – 8	-19.7	4.4	Wearable
[30]	15 × 40	FR-4	2.4/5.8	-25	2.5 / 4.2	WLAN
[31]	34 × 43	PTFE	1.4-4.9	-20	3.4	Bluetooth, WiMAX, WiFi
[32]	50 × 50	FR-4	2.4	-20	4	ISM
[33]	29.7× 38.3	FR-4	2.4	-20	6.74	WLAN
[34]	39.9× 47.4	RT 5870	2.4	-14	8.482	Radar
[35]	40 × 40FR-4	FR-4	2.4 / 5 / 13.4	-28	2.3 / 4.4 / 4.7	WLAN and Ku-band
[36]	70 × 70	Felt	2.4	-34	5.96	Wearable IoT
Our work	40 × 60	Felt	1.98–3.76 / 5.27–10.8	-45	7.85	Wearable IoT

IV. CONCLUSION

This study successfully developed a portable Internet of Things (IoT)-based system integrating a textile Coplanar Vivaldi Antenna (CVA) with an ESP32 microcontroller for early stunting detection. A parametric study was conducted on the CVA by varying the cavity radius and introducing a corrugated structure on the patch to achieve the desired operating frequency and antenna directivity. The CVA with a cavity radius of 3.5 mm achieved an impedance bandwidth of 133.17%. CVA type C produced the highest directivity, at 7.858 dBi; whereas, CVA type J demonstrated resonance frequencies at 2.39 GHz (–35.05 dB) and 5.87 GHz (–28.99 dB).

The system effectively integrates anthropometric data measurement and Z-score calculation based on weight, height, and head circumference data collected from a load cell, ultrasonic sensor, and flex sensor, respectively. The measurement error rates are very low: 0.08% for weight, 0.16% for height, and 0.13% for head circumference, meeting the standards required for health monitoring applications. The ESP-NOW protocol demonstrated strong performance, with an average latency of 82 ms in unobstructed conditions and 117 ms when physical obstacles were present. The system achieved a 93% data transmission success rate at a distance of 20 m.

Future enhancements may include integrating alternative communication protocols, such as LoRa or ZigBee, to extend the transmission range and using an alternative substrate antenna to improve the performance. Additional improvements could focus on reducing antenna dimensions to mitigate bending effects, lowering SAR values, employing alternate flexible substrates for optimal performance, and optimizing fabrication and measurement methods. Based on the obtained results, the system can be developed and recommended for portable stunting detection and IoT applications.

ACKNOWLEDGMENT

We would like to express our gratitude for the funding provided by the Indonesian Collaborative Research between State Universities with Legal Entities in East Java (ITS, Unair, UB, UM and UNESA) especially to Surabaya State University, under research contract number B/43905/UN38.III.1/ LK.04.00/2024.

REFERENCES

[1] K. C. Rao, D. Nataraj, K. S. Chakradhar, G. V. Ujwala, M. Lakshmunaidu, and H. S. Dadi, "Design of a Compact Millimeter Wave Antenna for 5G Applications based on Meta Surface Luneburg Lens," *Engineering, Technology & Applied Science Research*, vol. 15, no. 2, pp. 20722–20728, Apr. 2025, https://doi.org/10.48084/etasr.9349.

[2] T. D. T. Thanh, P. D. Quan, P. H. Phuc, and H. T. P. Thao, "A Penta-band Antenna using Symmetrical DGS for RF Energy Harvesting in IoT Applications," *Engineering, Technology & Applied Science Research*, vol. 15, no. 2, pp. 22028–22034, Apr. 2025, https://doi.org/10.48084/etasr.10138.

[3] A. Zandamela, N. Marchetti, M. J. Ammann, and A. Narbudowicz, "A Dual-Band Planar Antenna for Angle-of-Arrival Estimation in On-Body IoT Devices," *IEEE Internet of Things Journal*, vol. 12, no. 13, pp. 23921–23932, July 2025, https://doi.org/10.1109/JIOT.2025.3554738.

[4] P. Ramya *et al.*, "Enhancing 5G Performance: A Study of an MIMO Antenna with Elliptical Ring Polarization," *Engineering, Technology & Applied Science Research*, vol. 15, no. 1, pp. 19782–19787, Feb. 2025, https://doi.org/10.48084/etasr.9516.

[5] Y. E. Hachimi, E. M. Louragli, S. A. N. Arockiam, V. Subramanian, S. Das, and A. Farchi, "Design of a Miniaturized Dual-Band Antenna using Slotted Techniques for 2.45/5.8 GHz Microwave Band RFID Utilizations," *Engineering, Technology & Applied Science Research*, vol. 15, no. 1, pp. 20018–20023, Feb. 2025, https://doi.org/10.48084/etasr.9483.

[6] N. Nurhayati, N. N. Uma, M. Y. Farentina, R. D. Safitri, A. N. Dwi Nur Fahmi, and W. A. Godaymi Al-Tumah, "Wearable Monopole Textile Antenna for IoT Application," in *2024 International Conference on Computer Engineering, Network, and Intelligent Multimedia*, Surabaya, Indonesia, 2024, pp. 1–4, https://doi.org/10.1109/CENIM64038.2024.10882776.

[7] N. Nurhayati *et al.*, "Wearable Wideband Textile Coplanar Vivaldi Antenna for Medical and IoT Application," *Progress In Electromagnetics Research C*, vol. 148, pp. 145–156, Oct. 2024, https://doi.org/10.2528/pierc24080402.

[8] S. Agneessens, "Coupled Eighth-Mode Substrate Integrated Waveguide Antenna: Small and Wideband With High-Body Antenna Isolation," *IEEE Access*, vol. 6, pp. 1595–1602, 2018, https://doi.org/10.1109/ACCESS.2017.2779563.

[9] H. Kaur and P. Chawla, "Design and Evaluation of a Fractal Wearable Textile Antenna for Medical Applications," *Wireless Personal Communications*, vol. 128, no. 1, pp. 683–699, Jan. 2023, https://doi.org/10.1007/s11277-022-09973-8.

[10] U. Hasni and E. Topsakal, "Wearable Antennas for On-Body Motion Detection," in *2020 IEEE USNC-CNC-URSI North American Radio Science Meeting (Joint with AP-S Symposium)*, Montreal, Canada, 2020, pp. 1–2, https://doi.org/10.23919/USNC/URSI49741.2020.9321663.

[11] R. Huang, W. Xia, L. Xing, and F. Zhu, "A Dual-Band Footwear Textile Antenna for LoRa Off-Body Communication," in *2022 IEEE Conference on Antenna Measurements and Applications*, Guangzhou,

China, 2022, pp. 1–4, https://doi.org/10.1109/CAMA56352.2022.10002504.

[12] G. Li, Z. Tian, G. Gao, L. Zhang, M. Fu, and Y. Chen, "A Shoelace Antenna for the Application of Collision Avoidance for the Blind Person," *IEEE Transactions on Antennas and Propagation*, vol. 65, no. 9, pp. 4941–4946, Sept. 2017, https://doi.org/10.1109/TAP.2017.2722874.

[13] G. Bengloan, J. M. Felicio, C. A. Fernandes, A. Chousseaud, B. Froppier, and E. M. Cruz, "A Compact and Flexible Dual-Band Antenna for Near-Body Applications," in *2021 International Symposium on Antennas and Propagation*, Taipei, Taiwan, 2021, pp. 1–2, https://doi.org/10.23919/ISAP47258.2021.9614567.

[14] M. Hussain, W. A. Awan, S. M. Abbas, and Y. Zhu, "Design and development of low-profile polymer based broadband antenna for on-body applications," *Results in Engineering*, vol. 25, Mar. 2025, Art. no. 103818, https://doi.org/10.1016/j.rineng.2024.103818.

[15] W. M. Abdulkawi, A. Masood, N. Nizam-Uddin, and M. Alnakhli, "A Simulation Study of Triband Low SAR Wearable Antenna," *Micromachines*, vol. 14, no. 4, Apr. 2023, Art. no. 819, https://doi.org/10.3390/mi14040819.

[16] S. Jayant, G. Srivastava, and S. Kumar, "Quad-Port UWB MIMO Footwear Antenna for Wearable Applications," *IEEE Transactions on Antennas and Propagation*, vol. 70, no. 9, pp. 7905–7913, Sept. 2022, https://doi.org/10.1109/TAP.2022.3177481.

[17] S. Dey, M. S. Arefin, and N. C. Karmakar, "Design and Experimental Analysis of a Novel Compact and Flexible Super Wide Band Antenna for 5G," *IEEE Access*, vol. 9, pp. 46698–46708, 2021, https://doi.org/10.1109/ACCESS.2021.3068082.

[18] V. Kavitha, K. Malaisamy, T. Murugesh, and M. SenthilKumar, "Design and development of jeans textile antenna for wireless broadband applications," *Journal of Industrial Textiles*, vol. 53, Dec. 2023, Art. no. 15280837231215374, https://doi.org/10.1177/15280837231215374.

[19] M. A. Abdelghany, M. I. Ahmed, A. A. Ibrahim, A. Desai, and M. F. Ahmed, "Textile Antenna with Dual Bands and SAR Measurements for Wearable Communication," *Electronics*, vol. 13, no. 12, June 2024, Art. no. 2251, https://doi.org/10.3390/electronics13122251.

[20] H. Yalduz, B. Koç, L. Kuzu, and M. Turkmen, "An ultra-wide band low-SAR flexible metasurface-enabled antenna for WBAN applications," *Applied Physics A*, vol. 125, no. 9, Aug. 2019, Art. no. 609, https://doi.org/10.1007/s00339-019-2902-4.

[21] T. Siswati *et al.*, "Effect of a Short Course on Improving the Cadres' Knowledge in the Context of Reducing Stunting through Home Visits in Yogyakarta, Indonesia," *International Journal of Environmental Research and Public Health*, vol. 19, no. 16, Aug. 2022, Art. no. 9843, https://doi.org/10.3390/ijerph19169843.

[22] D. P. Hutabarat, W. Wijaya, and W. D. Wijaya, "Internet of things-based digital scale to detect stunting symptoms in babies under two years of age," *International Journal of Electrical and Computer Engineering*, vol. 14, no. 3, pp. 3467–3474, June 2024, https://doi.org/10.11591/ijece.v14i3.pp3467-3474.

[23] S. Wiyono *et al.*, "The role sanitation to stunting children age 6-35 months, Purwojati subdistrict, Banyumas district, Central Java, Indonesia," *International Journal Of Community Medicine And Public Health*, vol. 6, no. 1, pp. 82–88, Jan. 2019, https://doi.org/10.18203/2394-6040.ijcmph20185231.

[24] K. Widatama and P. W. Setyaningsih, "The Using Of Information Systems To Calculate Z-Score And To Determination Of Stunting Categories In Toddlers," *bit-Tech*, vol. 6, no. 2, pp. 152–160, Dec. 2023, https://doi.org/10.32877/bt.v6i2.1013.

[25] N. Nurhayati, F. Y. Zulkifli, E. Setijadi, B. E. Sukoco, M. N. M. Yasin, and A. M. De Oliveira, "Bandwidth, Gain Improvement, and Notched-Band Frequency of SWB Wave Coplanar Vivaldi Antenna Using CSRR," *IEEE Access*, vol. 12, pp. 16926–16938, 2024, https://doi.org/10.1109/ACCESS.2024.3359168.

[26] J. Tak, S. Woo, J. Kwon, and J. Choi, "Dual-Band Dual-Mode Patch Antenna for On-/Off-Body WBAN Communications," *IEEE Antennas and Wireless Propagation Letters*, vol. 15, pp. 348–351, June 2016, https://doi.org/10.1109/LAWP.2015.2444881.

[27] V. R. Preedy, Ed., *Handbook of Anthropometry: Physical Measures of Human Form in Health and Disease*. New York, NY, USA: Springer, 2012, https://doi.org/10.1007/978-1-4419-1788-1.

[28] Md. S. Rana, O. Islam, S. A. Shikha, and M. Faisal, "IoT Application using a Rectangular 2.4 GHz Microstrip Patch Antenna," in *2023 International Conference for Advancement in Technology*, Goa, India, 2023, pp. 1–4, https://doi.org/10.1109/ICONAT57137.2023.10080448.

[29] A. K. Biswas and U. Chakraborty, "A compact wide band textile MIMO antenna with very low mutual coupling for wearable applications," *International Journal of RF and Microwave Computer-Aided Engineering*, vol. 29, no. 8, July 2019, Art. no. e21769, https://doi.org/10.1002/mmce.21769.

[30] K.-L. Wong, H.-J. Chang, C.-Y. Wang, and S.-Y. Wang, "Very-Low-Profile Grounded Coplanar Waveguide-Fed Dual-Band WLAN Slot Antenna for On-Body Antenna Application," *IEEE Antennas and Wireless Propagation Letters*, vol. 19, no. 1, pp. 213–217, Jan. 2020, https://doi.org/10.1109/LAWP.2019.2958961.

[31] K. Mondal, A. Samanta, and P. P. Sarkar, "Compact Multiband Monopole Antenna for ISM Band 2.4 GHz, Bluetooth, WiMAX, WiFi Applications," *Wireless Personal Communications*, vol. 97, no. 1, pp. 181–195, Nov. 2017, https://doi.org/10.1007/s11277-017-4500-0.

[32] H. Li, J. Du, X.-X. Yang, and S. Gao, "Low-Profile All-Textile Multiband Microstrip Circular Patch Antenna for WBAN Applications," *IEEE Antennas and Wireless Propagation Letters*, vol. 21, no. 4, pp. 779–783, Apr. 2022, https://doi.org/10.1109/LAWP.2022.3146435.

[33] A. R. Nair, B. A. Singh, and S. S. Thakur, "Design of Rectangular Microstrip 4x2 Patch Array Antenna at 2.4 GHz for WLAN Application," in *2015 Second International Conference on Advances in Computing and Communication Engineering*, Dehradun, India, 2015, pp. 53–56, https://doi.org/10.1109/ICACCE.2015.18.

[34] H. Hadžić, W. Verzotti, Z. Blažević, and M. Škiljo, "2.4 GHz micro-strip patch antenna array with suppressed sidelobes," in *2015 23rd International Conference on Software, Telecommunications and Computer Networks (SoftCOM)*, Split, Croatia, 2015, pp. 96–100, https://doi.org/10.1109/SOFTCOM.2015.7314057.

[35] S. Lamultree, W. Thanamalapong, S. Dentri, and C. Phongcharoenpanich, "Tri-Band Bidirectional Antenna for 2.4/5 GHz WLAN and Ku-Band Applications," *Applied Sciences*, vol. 12, no. 12, June 2022, Art. no. 5817, https://doi.org/10.3390/app12125817.

[36] H. Lee and J. Choi, "A polarization reconfigurable textile patch antenna for wearable IoT applications," in *2017 International Symposium on Antennas and Propagation*, Phuket, Thailand, 2017, pp. 1–2, https://doi.org/10.1109/ISANP.2017.8228882.